Eur Radiol (2012) 22:1331–1340
DOI 10.1007/s00330-011-2370-5

MUSCULOSKELETAL

Metal artefact reduction in gemstone spectral imaging dual-energy CT with and without metal artefact reduction software

Young Han Lee · Kwan Kyu Park · Ho-Taek Song · Sungjun Kim · Jin-Suck Suh

Received: 10 August 2011 / Revised: 21 November 2011 / Accepted: 22 November 2011 / Published online: 4 February 2012

Abstract
Objective To assess the usefulness of gemstone spectral imaging (GSI) dual-energy CT (DECT) with/without metal artefact reduction software (MARs).
Methods The DECTs were performed using fast kV-switching GSI between 80 and 140 kV. The CT data were retro-reconstructed with/without MARs, by different displayed fields-of-view (DFOV), and with synthesised monochromatic energy in the range 40–140 keV. A phantom study of size and CT numbers was performed in a titanium plate and a stainless steel plate. A clinical study was performed in 26 patients with metallic hardware. All images were retrospectively reviewed in terms of the visualisation of periprosthetic regions and the severity of beam-hardening artefacts by using a five-point scale.
Results The GSI-MARs reconstruction can markedly reduce the metal-related artefacts, and the image quality was affected by the prosthesis composition and DFOV. The spectral CT numbers of the prosthesis and periprosthetic regions showed different patterns on stainless steel and titanium plates.
Conclusion Dual-energy CT with GSI-MARs can reduce metal-related artefacts and improve the delineation of the prosthesis and periprosthetic region. We should be cautious when using GSI-MARs because the image quality was affected by the prosthesis composition, energy (in keV) and DFOV. The metallic composition and size should be considered in metallic imaging with GSI-MARs reconstruction.
Key Points
- *Metal-related artefacts can be troublesome on musculoskeletal computed tomography (CT).*
- *Gemstone spectral imaging (GSI) with dual-energy CT (DECT) offers a novel solution*
- *GSI and metallic artefact reduction software (GSI-MAR) can markedly reduce these artefacts.*
- *However image quality is influenced by the prosthesis composition and other parameters.*
- *We should be aware about potential overcorrection when using GSI-MARs.*

Keywords Dual-energy CT · Computed tomography · Metallic artefacts

Y. H. Lee · H.-T. Song · S. Kim · J.-S. Suh (✉)
Department of Radiology, Research Institute of Radiological Science, Medical Convergence Research Institute, and Severance Biomedical Science Institute, Yonsei University College of Medicine,
250 Seongsanno, Seodaemun-gu,
Seoul 120-752, Republic of Korea
e-mail: jss@yuhs.ac

K. K. Park
Department of Orthopaedic Surgery,
Yonsei University College of Medicine,
250 Seongsanno, Seodaemun-gu,
Seoul 120-752, Republic of Korea

Introduction

As arthroplasty, a surgical replacement of the joint with an artificial joint, has been increasingly implemented to relieve joint pain [1], we occasionally meet arthroplasty failure, which requires revision. Computed tomography (CT) plays an important role in the postoperative evaluation of patients who were suspected of having metal prosthesis-related problems such as aseptic loosening, bone resorption or osteolysis, infection, dislocation, metallic failure or periprosthetic bone fracture [1–4]. However, the challenge is to improve image quality and diagnostic value in spite of metal-induced artefacts [2], such as beam-hardening artefacts and the photon starvation effects [3, 4]. X-ray beams with polychromaticity inherently cause metallic artefacts due to energy

averaging whereas a monochromatic X-ray spectrum shows fewer artefacts without an increment of the average energy.

For this reason, we investigated gemstone spectral imaging (GSI) using metal artefact reduction software (MARs) in dual-energy CT (DECT) in patients with metallic prosthesis o counteract the image-degrading effects of a polychromatic X-rays. The GSI-MARs technology has the potential to correct the metallic artefacts by segmentation and reconstruction based on a CT number threshold.

The purpose of this study was to assess the usefulness and diagnostic value of a metal artefact reduction CT protocol based on GSI DECT with/without MARs in minimising metallic artefacts in phantoms and in patients with orthopaedic prosthesis.

Materials and methods

Dual energy CT protocol

The CT examinations were preformed on a 64-channel Discovery CT750 HD (GE Healthcare, Milwaukee, WI, USA). The CT acquisition parameters were adjusted for the GSI-MARs protocol: GSI 17 preset protocol with beam collimation of 20 mm; slice thickness of 1.25 mm; rotation speed of 0.6 s; fast kV-switching between 80 and 140 kVp; current less than 640 mA; pitch 1.375:1; matrix 512×512; and pixel spacing 0.716×0.716–0.952×0.952 mm. All CT images were reconstructed both with/without MARs algorithm for comparison. Reconstructed parameters of the CT images in the patients included 70 keV, DFOV (displayed or reconstruction field-of-view) of 17.5–40 cm, slice thickness of 1.25 mm and standard reconstruction algorithms.

For phantom analyses, the CT raw data were retroreconstructed with/without MARs reconstruction and by different DFOVs. Post-processing was applied to generate synthesised monochromatic 40–140 keV images by using dedicated GSI viewer software (GSI viewer 2.00 and GE VolumeShare4 AW 4.4, GE Healthcare). The CT images were assessed digitally with a commercially available PACS workstation (Centricity® Radiology RA1000, GE Healthcare). A window width of 1200 HU and a window level of 200 HU were used.

Phantom analyses

A phantom study was performed for metal artefact evaluation of a titanium alloy plate (LCP Plate 4.5/5.0, Synthes, West Chester, PA, USA) and a stainless steel alloy plate (DHS® Plate 130° with barrel length 25 mm, Synthes), which are currently used for internal fixation of fractures (Fig. 1a). The plates were placed at the centre of a bottle filled with saline.

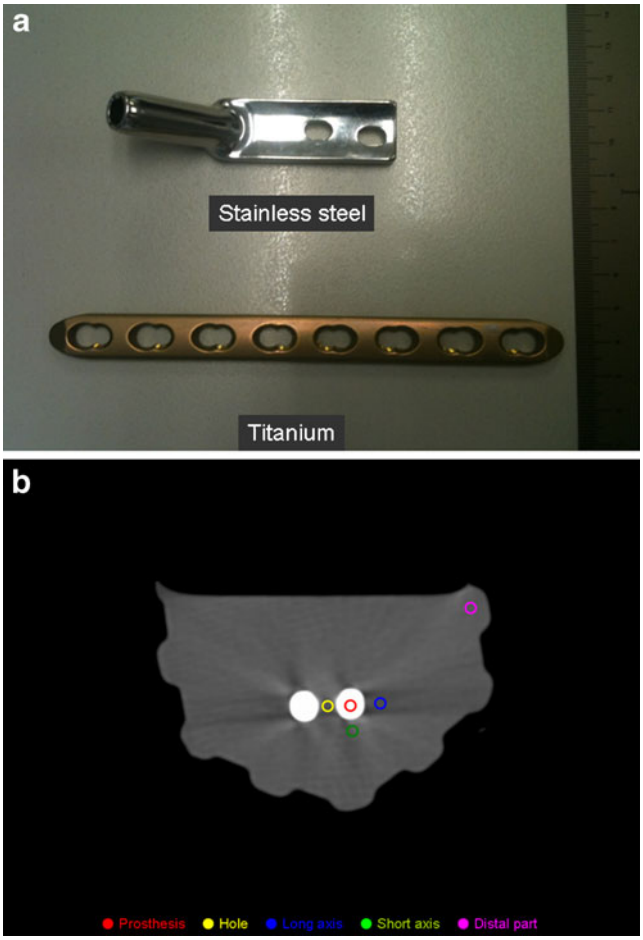

Fig. 1 Prosthesis phantoms. **a** Photograph of phantoms. A phantom study was performed by using a titanium alloy plate and a stainless alloy plate, which are currently used for internal fixation of fracture. **b** Regions of interest (ROIs) analysis. The ROIs of each prosthesis were measured on the prosthesis and on the periprosthetic regions of the prosthesis, the hole, the proximal part of the long axis, the proximal part of the short axis and the distal part with the same size (2×2 mm) and the same location

For the size analysis of prostheses, we measured the widths and the hole diameters of plates on CT images with and without MARs reconstruction: different DFOVs (10, 20, 30, 40 and 50 cm). For evaluation of the periprosthetic region and the regions of interest (ROIs) of the synthesised monochromatic CT images five different regions were identified: the prosthesis, the hole, the proximal part of the long axis, the proximal part of the short axis, and the distal part (3 cm away from the prosthesis) with the same size (2×2 mm) and same location, as illustrated in Fig. 1b. The average and standard deviation of CT numbers were measured and recorded for each ROI in the 40 keV to 140 keV images.

Clinical analyses

From November 2010 to May 2011, 26 consecutive patients with metallic prosthesis who had undergone the GSI-MARs

CTs were included and evaluated in the study: the patients had total hip arthroplasty (6), total knee arthroplasty (2), total shoulder arthroplasty (1), radial head arthroplasty (1), total ankle arthroplasty (1), tumour prosthesis (1), or fracture fixations with a plate, screw or pinning (14). The mean postoperative time interval between surgery and imaging was 31.6 months (range: 2–71 months). The mean age of 26 patients was 53.9 years (range: 27–79 years). Fourteen patients were male and 12 were female. The retrospective study protocol was approved by the institutional review board.

A total of 26 image sets with MARs and without MARs reconstruction of GSI CT images was retrospectively reviewed. All images were analysed in terms of the visualisation of the periprosthetic cortex, periprosthetic trabeculation, periprosthetic soft tissue and the severity of beam-hardening artefacts by two musculoskeletal radiologists (J.S.S., Y.H.L. with 25 and 5 years of experience in musculoskeletal radiology, respectively). The visualisation of the paired images was rated by using a five-point scale: 5, a fully diagnostic evaluation; 4, minor artefacts that do not affect diagnostic evaluation; 3 minor streaks without impact on the evaluation of the implant and the adjacent tissue; 2, restricted diagnostic interpretation; 1, insufficient diagnostic interpretation. The severity was rated by using a five-point scale: 5 being best to 1 being worst. The radiation doses were recorded according to the dose report from the CT console.

Statistical analysis

Paired Student's *t*-test was performed for the statistical analysis of the quantitative scales. A P value<0.05 was accepted as statistically significant. All statistical analyses were performed with SPSS software (version 18.0; SPSS Inc., Chicago, IL, USA).

Results

Phantom results

Generally, in a stainless steel phantom, the metallic artefacts were prominent but dramatically reduced by applying GSI-MARs reconstruction (Fig. 2). In a titanium phantom, the CT images showed less metallic artefacts on images with and without MARs (Fig. 2). The relationship between keV and the CT numbers (HU) of CT images with/without MARs is shown in Fig. 3.

Size measurements for prosthesis

The sizes of prostheses were measured on the CT images compared with the real size of the prostheses. The changes in keV could affect the size of the prosthesis. Generally, the size of the prosthesis tends to be small when the keV value is higher (Fig. 2a, Table 1). On GSI CT images without MARs, the size of stainless steel prostheses was overestimated owing to blurred contours resulting from beam-hardening artefacts. On GSI CT images with MARs, the size of titanium phantoms was underestimated (Fig. 2a).

In addition, it was noted that the selection of DFOV of GSI-MARs reconstruction affected the changes in the thickness and hole diameter of the prostheses. In MARs reconstruction, the image delineation of the prosthesis and periprosthetic region depended on the size of DFOV. As we chose DFOV with smaller MARs, the metal plates appeared as staircase features instead of a smooth contour (Fig. 2b). The measurements with different DFOVs are presented in Table 2.

CT numbers of prosthesis and periprosthetic region

The spectral CT numbers of the prosthesis and periprosthetic regions showed different patterns on stainless steel and titanium plates (Fig. 3). On GSI CT images without MARs, the maximal values of stainless and titanium plates are not different in 50–120 keV images. However, the titanium values decreased in the high (130 and 140 keV) energy images. On GSI CT images with MARs, the decreased HU values of the stainless steel phantom were shown in keV values above 70. On GSI CT images with MARs, the titanium phantom showed decreased CT numbers in inverse proportion to the keV values with large standard deviations. However, on GSI CT images without MARS, the stainless steel phantom did not show a decrease in HU values.

The imaging of the periprosthetic region was evaluated as the average and standard deviation of ROIs in four different regions. On GSI CT images without MARs, the optimal keV energy levels of periprosthetic image quality were determined: the CT numbers of periprosthetic regions are closest to 0 HU at 110 keV of stainless steel and 80 keV of titanium (Fig. 3). On GSI CT images with MARs, the periprosthetic regions of stainless steel phantom were relatively heterogeneous and some regions showed negative values (Fig. 3). These negative values of titanium were smaller than those of stainless steel (Fig. 2a).

Clinical results

In patients with metallic prosthesis, the GSI-MARs reconstruction showed marked improvement in image quality by effective metal artefacts reduction (Figs. 4, 5, 6 and 7, Table 3). The visualisation of the periprosthetic cortex, periprosthetic trabeculation, periprosthetic soft tissue and

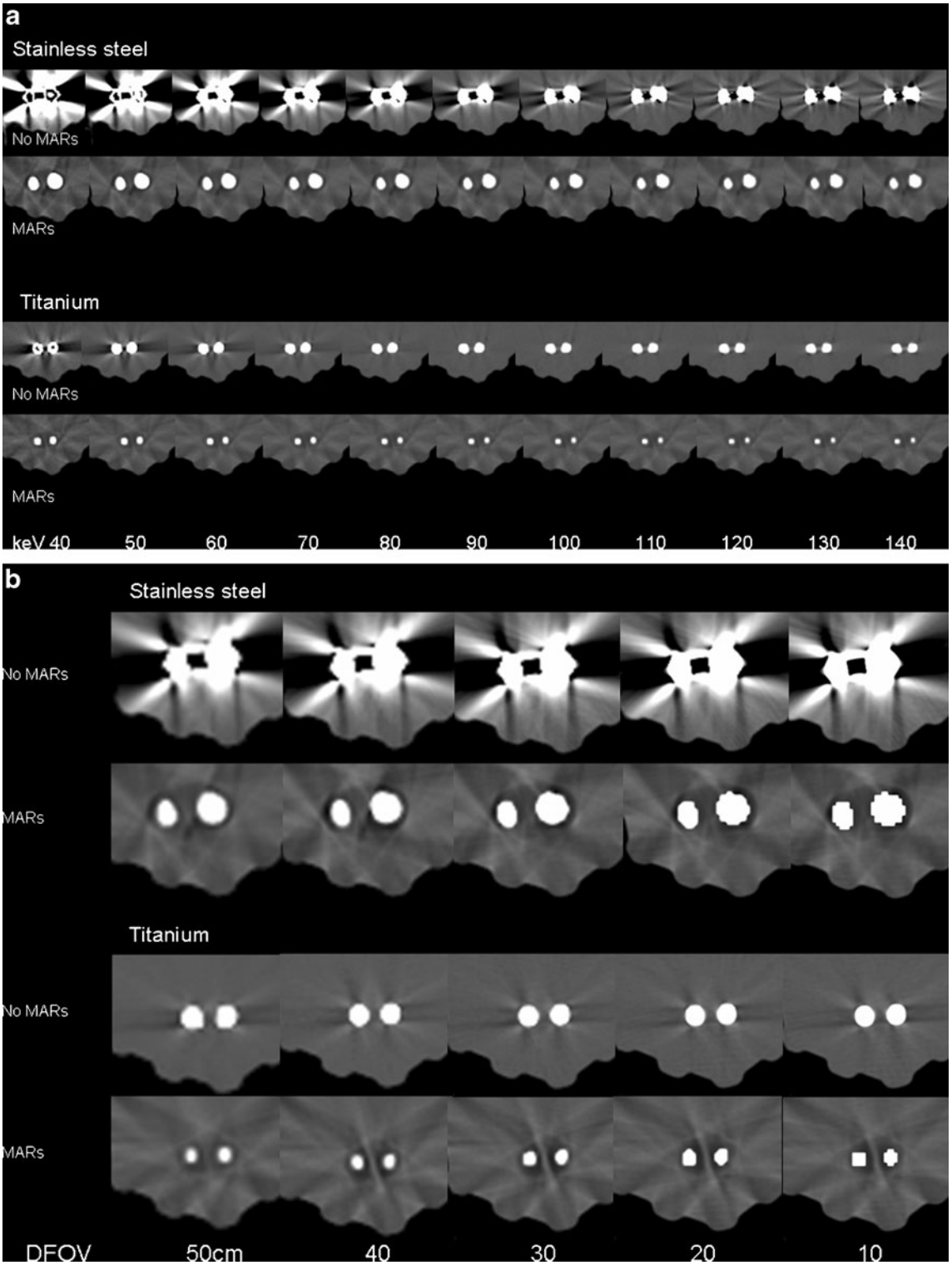

Fig. 2 GSI-MARs CT images of stainless steel and titanium phantoms with different serial keVs and different displayed fields-of view (DFOVs). **a** CT images with different serial keVs. The size is decreased in proportion to the keV values. **b** The CT images with different DFOVs. The prominence of staircase features is in inverse proportion to the size of DFOVs. In the titanium phantom, the background of the periprosthetic region shows heterogeneity

the severity of beam-hardening artefacts were significantly reduced on GSI CT images with MARs ($P<0.001$). These pathological features were surgically or arthroscopically confirmed ($n=17$).

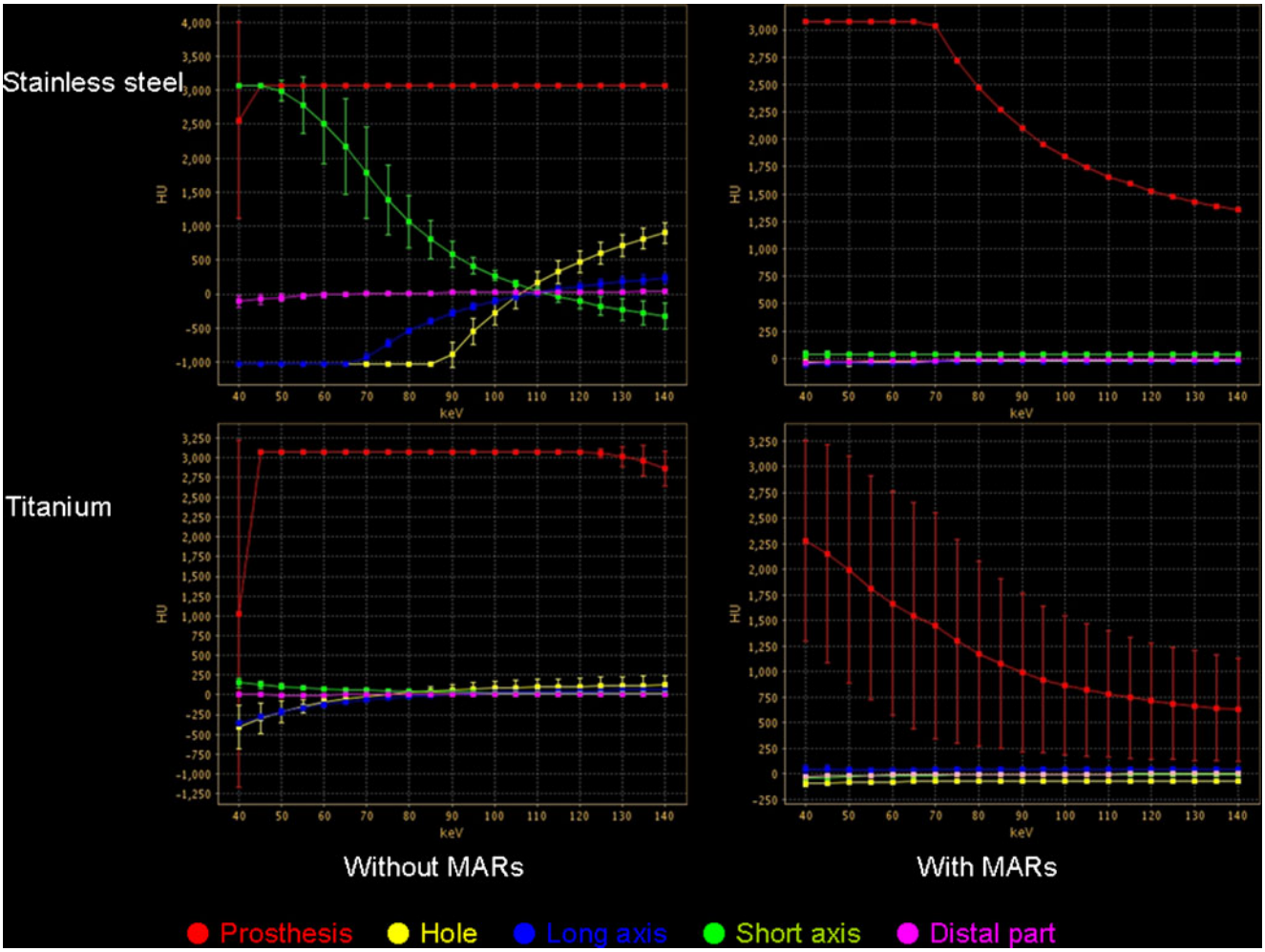

Fig. 3 Spectral HU analysis of phantoms. The spectral HU curves show the HU values of each prosthesis and each CT image with/without MARs

Table 1 Comparison of measurements of thickness and hole diameter of two plates among the different keV reconstructions

	Stainless steel				Titanium			
	Without MARs		With MARs		Without MARs		With MARs	
keV	Thickness (mm)	Hole (mm)	Thickness (mm)	Hole (mm)	Thickness (mm)	Hole (mm)	Thickness (mm)	Hole (mm)
40	23.11	5.47	19.81	5.51	15.36	3.81	13.02	5.48
50	22.81	5.77	19.61	5.71	15.34	4.11	12.73	5.48
60	22.55	5.69	19.51	5.95	15.34	4.11	12.67	5.68
70	21.80	5.71	19.48	6.01	15.33	4.20	12.52	5.97
80	21.53	5.25	19.42	6.49	15.31	4.20	12.50	6.05
90	21.27	5.12	19.07	6.59	15.26	4.20	12.34	6.18
100	21.21	5.11	19.05	6.78	15.16	4.20	12.28	6.76
110	21.16	5.11	19.01	6.88	15.11	4.20	12.22	6.85
120	21.13	5.10	18.78	6.98	15.06	4.30	12.11	7.15
130	21.22	5.10	18.67	7.07	15.04	4.49	11.86	7.15
140	21.32	5.10	18.67	7.17	15.01	4.49	11.86	7.35

DFOV Displayed or reconstruction field-of-view. The images are reconstructed from 30-cm DFOVs. The real size of thickness/hole diameter of stainless steel and titanium were 18/6 and 15/6 mm, respectively

Table 2 Comparison of measurements of thickness and hole diameter between CT without MARs and MARs reconstructions with different DFOVs

		Without MARs				With MARs			
		Thickness (mm)		Hole diameter (mm)		Thickness (mm)		Hole diameter (mm)	
	DFOV (cm)	80 keV	110 keV	80 keV	110 keV	80 keV	110 keV	80 keV	110 keV
Stainless steel	50	22.30	21.43	4.01	4.17	19.16	18.52	6.45	6.60
	40	22.01	21.21	5.23	5.45	19.40	19.21	6.47	7.06
	30	21.53	21.16	5.25	5.11	19.42	19.01	6.49	6.88
	20	21.57	20.60	5.33	4.72	20.47	19.82	5.50	5.59
	10	21.48	20.54	5.11	5.02	20.80	20.57	4.92	5.09
Titanium	50	15.84	15.51	3.37	3.92	12.85	12.48	6.36	6.60
	40	15.33	15.30	3.79	3.92	12.70	12.68	6.22	6.47
	30	15.31	15.11	4.20	4.20	12.50	12.22	6.05	6.85
	20	15.07	14.72	3.88	4.14	12.51	12.21	5.49	5.89
	10	14.93	14.73	3.96	4.16	12.69	12.36	6.00	6.11

The real size of the thickness/hole diameter of stainless steel and titanium were 18/6 and 15/6 mm, respectively

Like the phantom study (Fig. 2), the MARs-reconstructed GSI CT images showed the changes with different DFOVs in a patient with radial head prosthesis (Fig. 6). The acetabular component, ceramic liner, and the femoral head of the total hip arthroplasty were well delineated on GSI CT image with MARs, which showed changes with different keV values (Fig. 7).

The GSI CT with or without MARs does not increase the radiation dose for the same location. Hip imaging resulted in the volumetric CT dose index of 17.03 mGy with MARs, which is comparable to 16.57 mGy on 120-kVp conventional imaging without MARs.

Discussion

As arthroplasty, a surgical replacement of the joint with an artificial joint, has been increasingly implemented to relieve joint pain [1], we occasionally meet arthroplasty failure, which requires revisional arthroplasty. The causes of prosthetic failure include aseptic loosening, bone resorption or osteolysis, infection, dislocation, metallic failure, or periprosthetic bone fracture.

Plain radiography is a traditional imaging method for arthroplasty failure but it has low sensitivity and specificity [5, 6]. Arthrography can be used for detection of loosening

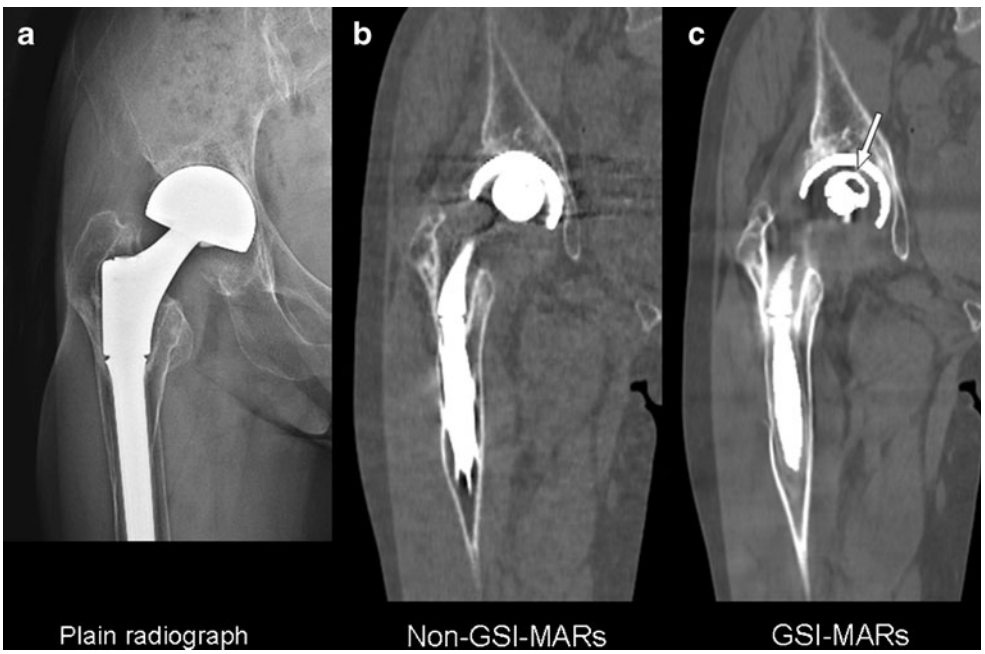

Fig. 4 A 68-year-old woman following bipolar hemiarthroplasty (stainless steel). The DFOV of CT images is 33.1 cm. **a** Hip arthroplasty did not show any information on the polyethylene liner. **b** The bone–prosthesis interfaces are not clearly delineated on CT without MARs at 70 keV. **c** The bone–prosthesis interfaces are clearly delineated on GSI-MARs CT at 70 keV. In particular, the gap, i.e. the polyethylene liner between the metallic cup and the femoral stem, is clearly delineated on the GSI-MARs CT (*arrow*). Superior migration of the femoral stem is seen. Polyethylene liner wearing was confirmed in the revisional operation

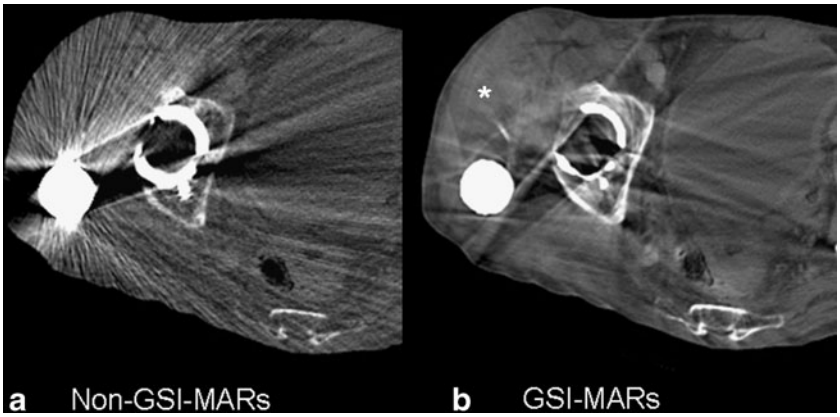

Fig. 5 A 70-year-old man after revisional total hip arthroplasty (titanium-aluminium alloy of the acetabular cup, polyethylene liner, the alumina-zirconia composite of the femoral head, and the titanium alloy of the femoral stem). The DFOV of the CT images is 40 cm. **a** CT image without MARs shows hip dislocation. The periprosthetic soft tissue and hip joint are not clearly delineated owing to beam hardening artefacts and photon starvation. **b** On the GSI-MARs CT image, metallic artefacts around the femoral head (alumina-zirconia composite) and acetabular cup (titanium-aluminium alloy) are reduced. Infected soft tissue and joint effusion (*asterisk*) are well delineated by showing visualisation of periprosthetic soft tissue. Septic arthritis was confirmed postoperatively

which is shown as leakage of contrast material around the prosthesis [7]. Joint aspiration is the method of choice when septic loosening is suspected although the technique is inherently invasive [8]. Alternatives are thought to be either CT or magnetic resonance imaging (MRI) in spite of troubling metal-related artefacts [9]. The degree of metallic artefacts depends on the thickness, density, orientation and geometry of the prosthesis and CT parameters including tube voltage, tube current and collimation [6, 10]. New CT technologies provide thinner slices, higher kVp or mAs, and a better reconstruction algorithm so that image quality can be improved [10–15]. However, some artefacts still remain problematic.

The metallic artefacts by photon starvation or beam hardening have limited the visualisation of metal devices and adjacent tissue [2]. Beam-hardening artefacts result from the X-ray polychromaticity which is one of the physical factors of X-ray beams. Low-energy X-rays of the polychromatic X-ray beams are preferentially attenuated through metallic prosthesis, which leads to an increase in the average energy of the beam. Contrary to the polychromatic X-ray, a monochromatic X-ray does not show an increase in the average energy and reduces the metallic artefacts. Monochromatic X-rays or monoenegetic extrapolation are being used in single or dual-energy CT [16–20].

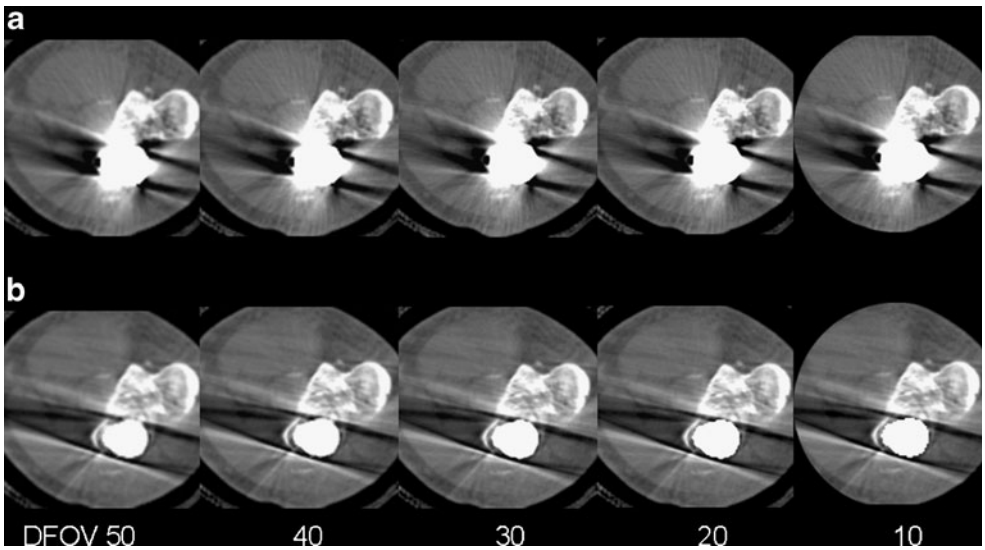

Fig. 6 A 35-year-old man after radial head arthroplasty with stainless steel. CT images were reconstructed with different DFOV values: 50, 40, 30, 20 and 10 cm. **a** CT image without MARs shows severe beam hardening artefacts and photon starvation around the prosthesis. The delineated prosthesis is not affected by the DFOVs. **b** The MARs CT image shows relatively less artefact by the correction of MARs technology. MARs-reconstructed radial head prosthesis shows the changes with different DFOVs. With a DFOV of 50 cm, the image is blurred because of the low spatial resolution. However, with a DFOV of 10 cm, the image shows prominent staircase features

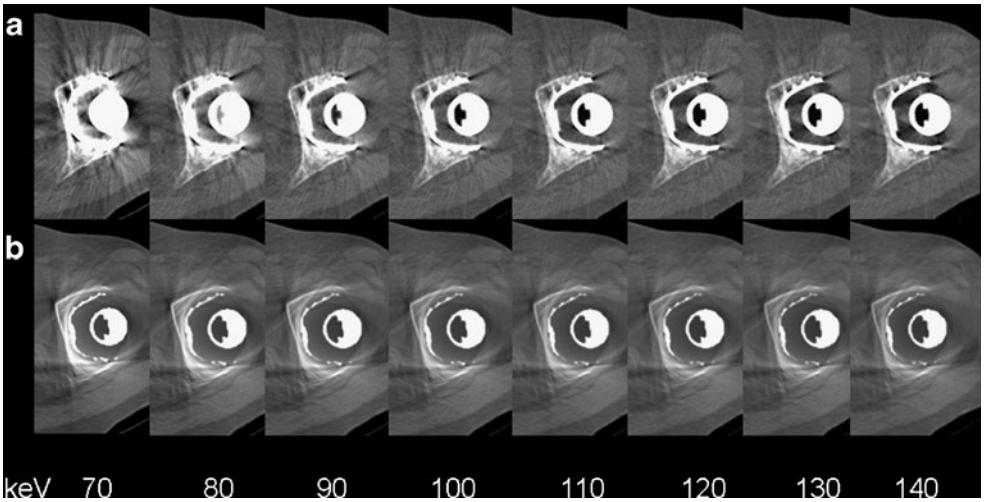

Fig. 7 A 63-year-old woman with total hip arthroplasty of the left hip: acetabular cup and femoral stem with stainless steel and femoral head with alumina ceramic. CT images were reconstructed with different keV values: 70, 80, 90, 100, 110, 120, 130 and 140 keV. Reconstructions with different DFOVs without MARs (**a**) and with MARs (**b**) showed the changes with different keV energy levels

The gemstone detector enabled the simultaneous dual-energy acquisition with an extremely fast speed. Gemstone spectral imaging (GSI) with fast kV switching between 80– and 140-kVp X-rays during a single rotation can produce

Table 3 Scores of the Image quality in GSI without and with MARs

		GSI without MARs				GSI with MARs			
n	Type	Cortex	Trabe-culation	Soft tissue	BHA	Cortex	Trabe-culation	Soft tissue	BHA
1	THA	1	5	1	5	3	5	2	4
2	Screw	4	5	4	4	3	4	3	4
3	Subtalar fusion	4	5	5	5	5	3	4	4
4	THA	2	5	1	3	2	4	2	5
5	Plate	5	4	5	5	5	4	3	4
6	THA	4	5	3	5	5	5	4	5
7	THA	2	5	2	5	2	5	2	5
8	IM nail	4	5	2	5	1	5	2	5
9	TKA	1	5	1	4	1	5	1	4
10	Pinning	4	5	2	2	4	4	3	4
11	Plate	4	5	3	5	2	5	2	5
12	Plate	2	5	3	5	3	5	1	4
13	IM nail	2	5	3	5	3	5	3	5
14	PLIF	3	5	3	5	2	5	2	5
15	Tumor prosthesis	3	5	3	5	2	2	2	2
16	THA	4	5	2	5	3	5	2	5
17	Plate	3	4	2	4	2	3	3	3
18	TSA	3	4	2	4	2	3	1	3
19	Plate	3	3	3	3	4	4	4	2
20	Plate	4	4	2	4	2	4	2	4
21	TAA	1	4	2	5	2	5	1	4
22	Plate	3	4	2	5	3	5	3	4
23	Screw	1	5	3	5	2	5	2	5
24	TKA	1	5	1	4	1	5	1	5
25	THA	2	5	2	5	3	5	3	5
26	RHR	1	5	2	4	1	3	2	5

THA Total hip arthroplasty, *IM nail* Intramedullary nail, *TKA* Total knee arthroplasty, *PLIF* Posterior lumbar interbody fixation, *TSA* Total shouder arthroplasty, *TAA* Total ankle arthroplasty, *RHR* Radial head replacement. Scores range from 1 to 5

consistent energy information of the monochromatic images. The two sets of low and high energy spectra generate the monochromatic images in a range of 40 to 140 keV through projection-based reconstruction to remove CT number shifts due to beam hardening [21, 22]. The advantages of the GSI include fewer beam hardening effects by reconstructing images at a chosen monochromatic energy.

Like other techniques for metal artefact reduction [19, 20], the metal artefact reduction software (MARs) built into a CT device capable of the GSI has the potential to further correct the metallic artefacts. In the GSI-MARs method, metal prosthesis can be segmented in a conventionally reconstructed image based on a CT number threshold. By forward projection, the metallic artefact-corrected image is then overlaid on the original image. The GSI-MARs can also replace the photon-starved regions with information derived from accurate projection measurements by using material decomposition on the corrected projections and monochromatic images. Therefore the GSI-MARs technology has the capability to improve image quality in patients with prosthesis (Figs. 4, 5, 6 and 7). The CT images still suffer from some metallic artefacts, but the overall image quality is improved. More importantly, the application of GSI-MARs does not need to increase the radiation dose contrary to the other techniques [3, 10]. This GSI-MARs technology can be applied to a number of kinds of reducing metal artefacts: sinuses or facial bones compromised by dental fillings, pelvic cavity compromised by a hip prosthesis, prosthetic joints such as total knee arthroplasty, vertebrae with interbody fusion devices, and CT-guided procedures such as arthrography or aspiration. Our results suggest that the GSI-MARs algorithm can reduce the metal artefact, allowing better delineation of the prosthesis itself and the periprosthetic region. This metallic artefact-reducing effect was greater in patients with larger prostheses such as total knee arthroplasty or femoral stem of total hip arthroplasty. The different pattern of the spectral analysis of prosthesis and periprosthetic regions (Fig. 3) can be utilised for the more sophisticated CT imaging in patients with metallic prosthesis in the future. We found some shortcomings of GSI-MARs, even though it was effective in metal artefact reduction. The GSI-MARs method makes prosthetic shapes and sizes variably by changing the DFOV or keV (Figs. 2, 6 and 7).

The optimal reconstruction protocol is required for the CT images with GSI-MARs. First, in our effort to optimise the reconstruction protocol for the CT images with GSI-MARs, we took it for granted that DFOVs are a determining factor. Adequate selection of DFOV improved the visualisation of prosthesis and the image quality of periprosthetic bone and soft tissue. The disfiguration we noticed is due to a larger reconstruction pixel in a smaller DFOV image. Hence, it may lead to wrong diagnosis by over-correction or mal-correction. A DFOV of less than 20 cm might be not recommended in this version of GSI-MARs (Figs. 2 and 6). Second, the image delineation of the prosthesis and periprosthetic region depends on the change in keV (Figs. 2 and 7). With our results we were unable to suggest the optimal keV for the prosthesis itself because of size overestimation on the GSI CT images or disfiguration on the GSI-MARs CT images. Heterogeneity around the prosthesis is another problem of the GSI-MARs CT images (Fig. 2). This heterogeneity is minimised at a certain keV energy level, which is the optimal keV for the periprosthetic region. Third, the composition of the prosthesis can influence the image quality. GSI-MARs CT is effective for the visualisation of stainless steel prosthesis. GSI-MARs may be not effective in metal artefact reduction for titanium prosthesis, although conventional CT causes the least artefact in titanium prostheses contrary to stainless steel, cobalt–chrome alloy, or cobalt [4, 23].

The question remained: Should postoperative CT be undertaken with GSI-MARs in all patients with a metallic device? We should be cautious when using GSI-MARs because the image quality was affected by the prosthesis composition, DFOV, and keV energy level (Figs. 2, 6 and 7). Table 4 presents a suggested imaging protocol optimised for patients with orthopaedic implants in terms of prosthesis composition, synthesised keV, and DFOV. We expect that the next version of GSI-MARs CT will be able to show more delicate correction of metallic artefacts.

In conclusion, dual-energy CT with GSI-MARs can reduce metal-related artefacts and improve the delineation of the prosthesis and periprosthetic region. We should be cautious when using GSI-MARs because the image quality was affected

Table 4 Suggested DECT parameters for metallic CT image

Parameter	Value
FOV	Medium or Large
Beam collimation (mm)	[a] 20
Pitch	[a] 1.375:1
kV	[b] 80 and 140
mA	[b] Less than 600
Matrix	512×512
Reconstruction (keV)	[c] 80 and 110
Reconstruction thickness (mm)	1
Reconstruction DFOV (cm)	20–35
Reconstruction plane	Axial, coronal and sagittal
Window level	200
Window width	1,200

[a] Default values of GSI preset 17

[b] Default values of GSI-MARs CT

[c] 80 keV for titanium and 110 keV for stainless steel

FOV Field-of-view, *DFOV* Displayed or reconstruction field-of-view

by the prosthesis composition and DFOV. The metallic composition and size should be considered in metallic imaging with GSI-MARs reconstruction. GSI-MARs may be not effective in metal artefact reduction for titanium prosthesis.

Acknowledgement This study was supported by a faculty research grant of Yonsei University College of Medicine (6-2008-0223).

References

1. National Hospital Discharge Survey: survey results and products. Atlanta: Centers for Disease Control and Prevention, 2009. (Accessed May 5, 2011, at http://www.cdc.gov/nchs/nhds/nhds_products.htm. .
2. White LM, Buckwalter KA (2002) Technical considerations: CT and MR imaging in the postoperative orthopedic patient. Semin Musculoskelet Radiol 6:5–17
3. Barrett JF, Keat N (2004) Artifacts in CT: recognition and avoidance. Radiographics 24:1679–1691
4. Haramati N, Staron RB, Mazel-Sperling K et al (1994) CT scans through metal scanning technique versus hardware composition. Comput Med Imaging Graph 18:429–434
5. Love C, Marwin SE, Palestro CJ (2009) Nuclear medicine and the infected joint replacement. Semin Nucl Med 39:66–78
6. Buck FM, Jost B, Hodler J (2008) Shoulder arthroplasty. Eur Radiol 18:2937–2948
7. Gelman MI, Coleman RE, Stevens PM, Davey BW (1978) Radiography, radionuclide imaging, and arthrography in the evaluation of total hip and knee replacement. Radiology 128:677–682
8. Phillips WC, Kattapuram SV (1983) Efficacy of preoperative hip aspiration performed in the radiology department. Clin Orthop Relat Res 141–146
9. Young SW, Muller HH, Marshall WH (1983) Computed tomography: beam hardening and environmental density artifact. Radiology 148:279–283
10. Lee MJ, Kim S, Lee SA et al (2007) Overcoming artifacts from metallic orthopedic implants at high-field-strength MR imaging and multi-detector CT. Radiographics 27:791–803
11. Watzke O, Kalender WA (2004) A pragmatic approach to metal artifact reduction in CT: merging of metal artifact reduced images. Eur Radiol 14:849–856
12. Li H, Yu L, Liu X, Fletcher JG, McCollough CH (2010) Metal artifact suppression from reformatted projections in multislice helical CT using dual-front active contours. Med Phys 37:5155–5164
13. Li H, Yu L, Liu X, McCollough CH (2009) Metal artifact suppression from reformatted projections in multi-slice helical CT using dual-front active contours. Conf Proc IEEE Eng Med Biol Soc 2009:993–996
14. Yu L, Li H, Mueller J et al (2009) Metal artifact reduction from reformatted projections for hip prostheses in multislice helical computed tomography: techniques and initial clinical results. Invest Radiol 44:691–696
15. Link TM, Berning W, Scherf S et al (2000) CT of metal implants: reduction of artifacts using an extended CT scale technique. J Comput Assist Tomogr 24:165–172
16. Montner SM, Lehr JL, Oravez WT (1987) Quantitative evaluation of a dual energy CT system. J Comput Assist Tomogr 11:144–150
17. Dilmanian FA (1992) Computed tomography with monochromatic x rays. Am J Physiol Imaging 7:175–193
18. Dilmanian FA, Wu XY, Parsons EC et al (1997) Single-and dual-energy CT with monochromatic synchrotron x-rays. Phys Med Biol 42:371–387
19. Bamberg F, Dierks A, Nikolaou K, Reiser MF, Becker CR, Johnson TR (2011) Metal artifact reduction by dual energy computed tomography using monoenergetic extrapolation. Eur Radiol 21:1424–1429
20. Boas FE, Fleischmann D (2011) Evaluation of two iterative techniques for reducing metal artifacts in computed tomography. Radiology 259:894–902
21. Lin XZ, Miao F, Li JY, Dong HP, Shen Y, Chen KM (2011) High-definition CT Gemstone spectral imaging of the brain: initial results of selecting optimal monochromatic image for beam-hardening artifacts and image noise reduction. J Comput Assist Tomogr 35:294–297
22. Zhang D, Li X, Liu B (2011) Objective characterization of GE discovery CT750 HD scanner: gemstone spectral imaging mode. Med Phys 38:1178–1188
23. Douglas-Akinwande AC, Buckwalter KA, Rydberg J, Rankin JL, Choplin RH (2006) Multichannel CT: evaluating the spine in postoperative patients with orthopedic hardware. Radiographics 26:S97–S110